ELSEVIER

Chemical Engineering Journal 132 (2007) 183–193

Chemical Engineering Journal

www.elsevier.com/locate/cej

Mathematical modeling of multiple solutes system for reverse osmosis process in palm oil mill effluent (POME) treatment

A.L. Ahmad *, M.F. Chong, S. Bhatia

School of Chemical Engineering, Engineering Campus, Universiti Sains Malaysia, Seri Ampangan, 14300 Nibong Tebal, Penang, Malaysia

Received 16 August 2006; received in revised form 4 December 2006; accepted 13 December 2006

Abstract

A membrane transport model suitable for the multiple solutes system in reverse osmosis is developed for unsteady-state simulation and prediction of membrane filtration dynamics in terms of permeate flux and concentration of each solute. This model is based on coupling the concentration polarization model using unsteady-state differential material balance and extended Spiegler-Kedem model. This model is characterized by the parameters solute diffusivity in the concentration polarization layer (D_{bi}), reflection coefficient (σ_i), osmotic constant (a_i), hydraulic permeability constant (L_p), mass transfer coefficient (k_i) and solute permeability coefficient (P_{ii}). These parameters are estimated by using the Levenberg–Marquardt method coupled with the Gauss–Newton algorithm using the experimental data. The experimental data were obtained from the treatment of pretreated palm oil mill effluent (POME) as a feed in the pilot plant scale reverse osmosis system. The pretreated POME composed of a ternary system with the solutes of carbohydrate constituents, protein and ammoniacal nitrogen. The simulation results show a good agreement with the experimental data. The proposed model is suitable for predicting the performance of multiple solutes in a reverse osmosis process. The concentration of each solute present is correlated with the COD of the permeate stream.

Keywords: Multiple solutes; Reverse osmosis; Concentration polarization; Spiegler-Kedem; POME

1. Introduction

Palm oil mill effluent (POME) is the thick brownish viscous liquid waste discharged from the palm oil mills during the extraction of palm oil from the fruits and is non-toxic but has an unpleasant odor. It is predominantly organic in nature and highly polluting [1]. POME is a colloidal suspension of 95–96% water, 0.6–0.7% oil and 4–5% total solids including 2–4% suspended solids originating from mixture of a sterilizer condensate, separator sludge and hydrocyclone wastewater [2].

The reverse osmosis membranes have been widely used for desalination of seawater and brackish waters to produce high quality drinking water [3,4]. Recently, the application of reverse osmosis membranes has been extended to the separation of organic solutions. Several researchers successfully applied the reverse osmosis membranes in the removal of viruses, endocrine disrupting compounds (EDCs), pharmaceutically active compounds (PhACs), natural organic matters (NOM), dyes and fluorides [5–7].

The hybrid processes, in which the reverse osmosis membranes are combined with conventional processes, are used in various applications [8]. The reverse osmosis membranes gave a 99% of COD removal in the treatment of chemical–biological treated dairy effluent [9]. Integrated system of activated sludge-reverse osmosis in the treatment of the wastewater from the meat industry enabled the water to be recovered and reused in the production cycle [10]. Qin et al. [11] reported that the reverse osmosis membranes successfully reclaimed the high-grade water (NEWater) from the secondary treated sewage effluent for its usage in the electronics industry.

Studies on the transport modeling of the multiple solutes system for organic solutions have been reported in the literature. Darnon et al. [12], combined the film model and Spiegler-Kedem model to evaluate the transport of proteins in complex biological solutions. Mi et al. [5] developed a spiral-wound element model to investigate the passage of viruses through imperfect spiral wound reverse osmosis membranes. A model based on the solution diffusion mass transport theory, concentration polarization and pressure dependent dynamic membrane resistance was

* Corresponding author. Tel.: +60 4 5937788; fax: +60 4 5941013.
E-mail address: chlatif@eng.usm.my (A.L. Ahmad).

1385-8947/$ – see front matter © 2006 Elsevier B.V. All rights reserved.
doi:10.1016/j.cej.2006.12.022

Nomenclature

a_i	osmotic constant (m^3 Pa/g)
b_i	dimensionless coefficient of Eq. (10)
C_{bi}	solute bulk feed concentration (kg/m^3)
C_{bi_0}	initial solute bulk feed concentration (kg/m^3)
C_i	solute concentration (kg/m^3)
$\bar{C}_i$	average value of solute bulk feed and permeate concentration (kg/m^3)
C_{pi}	solute permeate concentration (kg/m^3)
C_{wi}	solutes wall concentration (kg/m^3)
d_h	hydraulic diameter (m)
D_{bi}	solute diffusivity in the concentration polarization layer (m^2/s)
F_i	product constant of Eq. (7)
J_v	volumetric flux of permeate (m^3/m^2 s)
k	mass transfer coefficient (m/s)
L	phenomenological coefficient
L_p	hydraulic permeability constant (m/Pa s)
m_i	solute molar mass (g/mol)
ΔP	trans-membrane pressure (bar)
P_{ii}	solute permeability coefficient solute i with the consideration of the interaction of solute i (m/s)
P_{ij}	solute permeability coefficient of solute i with the consideration of the interaction of solute j (m/s)
R_g	ideal gas constant (8.314 m^3 Pa/mol K)
R_i	intrinsic rejection of the solute
R_o	observed rejection
t	filtration time (s)
T	operating temperature (K)
U	superficial velocity (m/s)
x	coordinate perpendicular to the membrane
x^*	dimensionless boundary layer thickness

Greek letters

α_i	dimensionless constant of Eq. (16)
β_i	dimensionless constant of Eq. (16)
δ_{pol}	thickness of concentration polarization layer (m)
μ	viscosity (Pa s)
σ_i	reflection coefficient

developed to predict the performance of reverse osmosis for mixed salt and dye solutions [13]. Pastagia et al. [14] developed an unsteady-state mass transfer model for binary solute system composed of reactive black dye and reactive red dye.

In the above studies, most of the transport models for reverse osmosis are only suitable for steady-state condition. However, one of the most important drawbacks of the membrane separation process is the decline in flux due to concentration polarization. It reduces the production rate and increases complexity of membrane filtration operation since the system has to be stopped frequently to restore the flux by back flushing. This phenomenon also results in difficulty regarding the simulation of time dependant permeate flux and rejection at any operating condition. Hence, modeling of the concentration polarization phenomenon to predict the unsteady-state permeate flux and rejection is necessary for the design of any membrane separation process. The unsteady-state transport model developed by Pastagia et al. [14] is only suitable for binary system. On the contrary, industrial processes apply to complex solutions, which their compositions are hardly known compared to those synthetic solutions treated in the theoretical studies.

The objective of the present study is to propose a method to depict solutes and water transfer through reverse osmosis membranes when the feed solution (POME) contain complex organic matters by using unsteady-state simulation with coupled model of concentration polarization and extended Spiegler-Kedem model where solute–solute interactions are considered. The measurable objectives are:

(1) To propose a membrane transport model for multiple solutes system in reverse osmosis based on the coupled model of concentration polarization using unsteady-state differential material balance and extended Spiegler-Kedem model.
(2) To estimate the parameters of the model from the experimental data obtained from the reverse osmosis system.
(3) To validate the proposed model by comparing the simulated results with the experimental results.
(4) To correlate the concentration of each solute with the chemical oxygen demand (COD) of the permeate.

2. Theory

A serious limitation in the operation of the reverse osmosis process is the progressive deterioration in permeate flux with time due to the fouling phenomena of concentration polarization. Unsteady-state modeling in permeation flux and quality is important to accomplish efficient and economical process design, achieving effective up-scaling to full scale operation [15]. The overall task of simultaneously predicting the unsteady-state permeation flux and rejection of organics solutes of a mixture involves a coupled solution of two transport models. The first model describes the transport phenomena in the concentration polarization boundary layer on the feed side adjacent to the membrane, while the second model deals with transport phenomena of organic solutes across the membrane based on extended Spiegler-Kedem model yielding the intrinsic rejection of the organic solutes. The extended Spiegler-Kedem model is coupled to the model of concentration polarization through the membrane surface boundary conditions. The coupled solution of the extended Spiegler-Kedem model and the model of concentration polarization provides simultaneous predictions of the unsteady-state permeate flux and observed rejection of the organic solutes.

2.1. Concentration polarization of multiple solutes system

In the multiple solutes system of reverse osmosis, there are $(n+1)$ components system with n solutes ($i = 1, 2, 3, \ldots, n$) in a solvent (e.g., water). The concentration polarization layer adjacent to the membrane surface can be schematically represented as shown in Fig. 1. Within the concentration polarization layer,

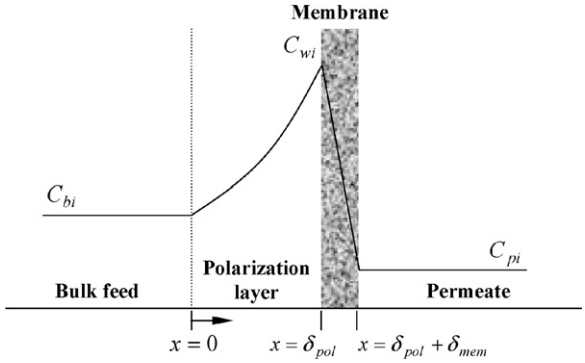

Fig. 1. Schematic of a concentration polarization boundary layer. The notation C_{wi} is the solutes wall concentration and C_{pi} is the solutes permeate concentration.

the governing equation for the concentration of each solute i is based on the unsteady-state differential material balance [16].

$$\frac{\partial C_i}{\partial t} = -J_v \frac{\partial C_i}{\partial x} + D_{bi} \frac{\partial^2 C_i}{\partial x^2} \tag{1}$$

where J_v is the volumetric flux of permeate, C_i the solute concentration in the polarization layer, D_{bi} the solute diffusivity in the concentration polarization layer, t the filtration time and x is the coordinate perpendicular to the membrane as shown in Fig. 1.

Eq. (1) is solved with the following initial and boundary conditions.

$$t = 0, \quad 0 \le x \le \delta_{pol}, \quad C_i = C_{bi_0} \tag{2a}$$

$$t \succ 0, \quad x = 0, \quad C_i = C_{bi} \tag{2b}$$

$$t \succ 0, \quad x = \delta_{pol} \quad J_v C_i|_{x=\delta_{pol}} = D_{bi} \frac{\partial C_i}{\partial x}\bigg|_{x=\delta_{pol}} \tag{2c}$$

where δ_{pol} is the thickness of concentration polarization layer, C_{bi_0} the initial solutes bulk feed concentration and C_{bi} is the solutes bulk feed concentration.

2.2. Transport of organic solutes for multiple solutes system

The extended Spiegler-Kedem model of multiple solutes is derived from the irreversible thermodynamics where solute–solute interactions are considered [17,18]. In this model, the membrane is treated as a black box in which relatively slow processes proceed near the equilibrium without specific transport mechanism and structure of the membrane. The model simply considers that the fluxes of solutes and solvent are directly related to the chemical potential differences between the two sides of the membrane. The chemical potential gradient is caused either by concentration or pressure gradient [19]. The transport equation for the volumetric flux of permeate, J_v with n solutes where $i = 1, 2, 3, \ldots, n$ can be written as [17]

$$J_v = L_p \left[\Delta P - \sum_{i=1}^{n} \sigma_i a_i R_i C_{wi} \right] \tag{3}$$

The term L_p is the hydraulic permeability constant, σ_i the reflection coefficient, ΔP the trans-membrane pressure, C_{wi} the solute i wall concentration, a_i the osmotic constants [14] and the term R_i is the intrinsic rejection of the solutes and is defined as

$$R_i = 1 - \frac{C_{pi}}{C_{wi}} \tag{4}$$

where C_{pi} is the solute i permeate concentration.

The osmotic constant is defined as [17]

$$a_i = \frac{R_g T}{m_i} \tag{5}$$

where m_i is the solute i molar mass, R_g the ideal gas constant and T is the operating temperature. For the multiple solutes system where $i = 1, 2, 3, 4, \ldots, n$ and $[j = 1, 2, 3, 4, \ldots, n$ and $j \neq i]$, the solute permeate concentration is given by [17]

$$\frac{R_{oi}}{1 - R_{oi}} = \frac{\sigma_i (1 - F_i)}{1 - \sigma_i} \exp \frac{-J_v}{k_i} \tag{6}$$

where

$$F_i = \exp \left[\frac{-J_v (1 - \sigma_i)}{P_{ii}} \left(1 + \sum_{j=1}^{n} A_j \right) \right] \tag{7}$$

$$A_j = \frac{P_{ij} (C_{pj} - C_{bj}) \exp(J_v / k_j)}{J_v [C_{pi} - (1 - \sigma_i) \bar{C}_i]} \tag{8}$$

The term k is the mass transfer coefficient and $\bar{C}_i$ is the average value of the bulk feed and permeate solute concentrations. The term R_o is the observed rejection and is defined as

$$R_{oi} = 1 - \frac{C_{pi}}{C_{bi}} \tag{9}$$

The term P_{ii} is the solute permeability coefficient of solute i with the consideration of the interaction of solute i and is defined as

$$P_{ii} = \left(\frac{L_{wi}^2}{L_{ww} C_i} - \frac{L_{ii}}{C_i} \right) \frac{R_g T}{l m_i} \tag{10}$$

where the L_{ii} and L_{ww} is the straight phenomenological coefficient for solute i and solvent, respectively, the L_{wi} is the cross phenomenological coefficient of solvent–solute i, and l is the membrane thickness.

The term P_{ij} is the solute permeability coefficient of solute i with the consideration of the interaction of solute j and is defined as

$$P_{ij} = \left(\frac{L_{wi} L_{wj}}{L_{ww} C_j} - \frac{L_{ij}}{C_j} \right) \frac{R_g T}{l m_j} \tag{11}$$

The L_{wj} and L_{ij} is the cross phenomenological coefficient of solvent–solute j and solute i–solute j, respectively.

Solving the Eqs. (1)–(9) simultaneously, the solute wall concentrations, permeate flux and permeate concentrations for each solute can be predicted once the parameters of D_{bi}, σ_i, a_i, L_p, k_i, P_{ii} and P_{ij} are determined.

In the application of membrane technology in the wastewater treatment, the chemical oxygen demand (COD) is often used to monitor the efficiency of the treatment method. The COD is closely related to the concentrations of solute in the system. A

correlation is used in the present studies to relate the concentrations of all solutes in the system with the COD as follows [20]:

$$C_{\mathrm{COD}} = \sum_{i=1}^{n} b_i C_i \quad \text{for} \quad i = 1, 2, 3, \ldots, n \tag{12}$$

where the term C_{COD} is the total COD concentration in the system, C_i the concentration of solute i in the system and b_i is the dimensionless coefficient.

2.3. Solution of the governing equations

Eq. (1) of unsteady-state differential material balance describing the concentration polarization is nondimensionalized by introducing the dimensionless variables as follows:

$$C_i^* = \frac{C_i}{C_{\mathrm{b}i_0}}, \quad C_{\mathrm{b}i}^* = \frac{C_{\mathrm{b}i}}{C_{\mathrm{b}i_0}}, \quad t_i^* = \frac{t}{\tau_i}, \quad \tau_i = \frac{\delta_{\mathrm{pol}}^2}{D_{\mathrm{b}i}},$$

$$x^* = \frac{x}{\delta_{\mathrm{pol}}}$$

Thus, Eq. (1) becomes

$$\frac{\partial C_i^*}{\partial t_i^*} = -\frac{J_{\mathrm{v}}\delta_{\mathrm{pol}}}{D_{\mathrm{b}i}}\frac{\partial C_i^*}{\partial x^*} + \frac{\partial^2 C_i^*}{\partial x^{*2}} \tag{13}$$

The boundary conditions of Eqs. (2b) and (2c) can be rewritten as:

$$x^* = 0, \quad C_i^* = C_{\mathrm{b}i}^* \tag{14a}$$

$$x^* = 1, \quad C_i^*\big|_{x^*=1} = \frac{D_{\mathrm{b}i}}{J_{\mathrm{v}}\delta_{\mathrm{pol}}}\frac{\partial C_i^*}{\partial x^*}\bigg|_{x^*=1} \tag{14b}$$

Eqs. (13) and (14) are solved numerically by employing finite element method [21]. The dimensionless boundary layer thickness, x^* was discretized into 100 equally spaced intervals with 101 nodes such that $x^* = 0$ corresponded to the first node and $x^* = 1$ corresponded to the 101th node. The Eq. (13) is converted into a set of ordinary differential equations (ODEs) using second-order accurate spatial discretization method based on the set of nodes [22]. The resulting ODEs are then solved numerically using backward differentiation method [21]. Solving the ODEs provides the profile of C_i and $C_{\mathrm{w}i}$ against t and x. The values of $C_{\mathrm{w}i}$ against t are used to calculate the unsteady-state permeate flux and intrinsic rejection (quality) by using Eqs. (3)–(9).

The overall model couples the extended Spiegler-Kedem model with the model of concentration polarization by the intrinsic rejections and the wall concentrations of each solute. The coupling between the two models thus requires an iterative solution algorithm which is solved using the software package of Matlab 7.0 as outlined below (Fig. 2):

1. The feed concentrations of each solute and operating parameters are the independent variables. The membrane parameters σ_i, a_i, $D_{\mathrm{b}i}$, L_{p}, k_i, P_{ii} and P_{ij} are obtained from the parameter estimation using the experimental data.

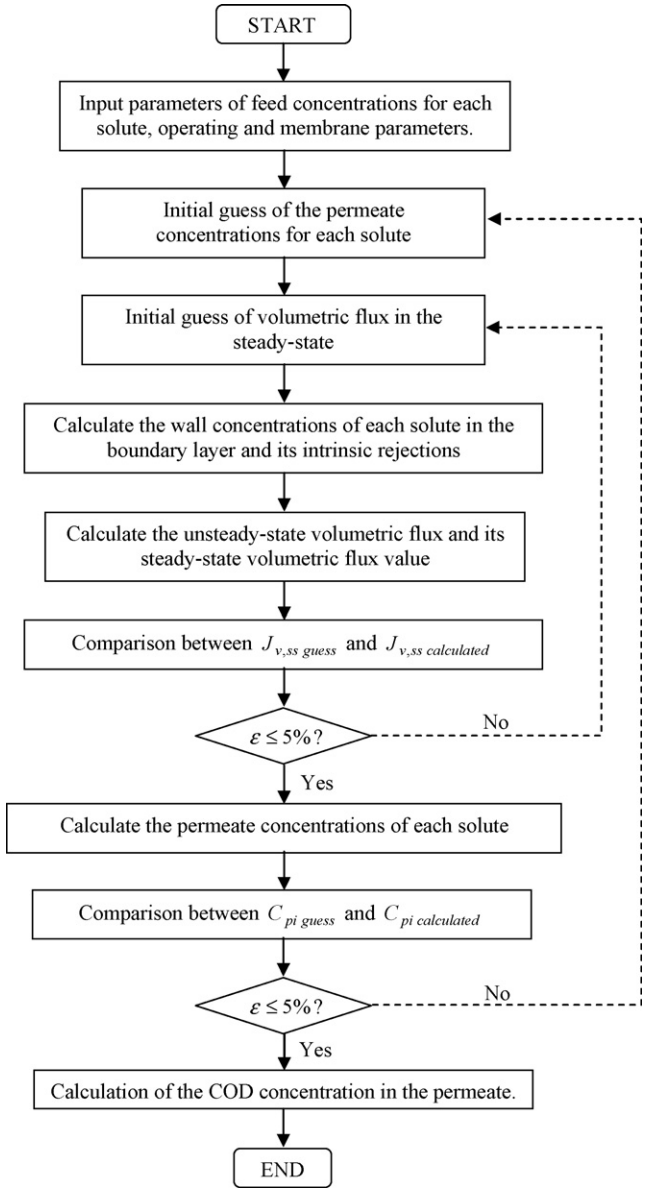

Fig. 2. Flow diagram of the algorithm for solution of the governing equations.

2. Since the procedure is iterative, the initial estimate of the permeate concentrations of each solute and volumetric flux are required. The wall concentrations profile of each solute against time was obtained from the model of concentration polarization of Eq. (13) by using the initial and boundary condition of Eqs. (2a), (14a) and (14b). The intrinsic rejections, R_i profile of each solute against time are calculated from Eq. (4).
3. Using the calculated values of the wall concentrations and intrinsic rejections profile of each solute against time, the unsteady-state volumetric flux is calculated by using Eq. (3). The volumetric flux at steady-state is obtained when the calculated value of volumetric flux remained constant over a period of time.
4. The permeate concentrations for each solute are obtained by solving the set of Eqs. (6)–(8) simultaneously when the comparison between the calculated value and the initial guess

of volumetric flux at steady-state show an error less than 5%.
5. The calculation is terminated when the error between the initial guess of the permeate concentrations for each solute and the calculated value is less than 5%.
6. The total COD concentration of permeate is calculated from the Eq. (12).

2.4. Parameter estimation method

The hydraulic permeability coefficient, L_p can be determined by running the experiment with deionized water at increasing pressure and the other parameters of σ_i, D_{bi}, P_{ii} and P_{ij} can be estimated using non-linear parameter estimation technique with Levenberg–Marquardt with Gauss–Newton algorithm [23].

The mass transfer coefficients for each solute, k_i are determined using velocity variation method [24] as follows:

$$\ln\left(\frac{1}{R_{oi}}-1\right)=\ln\left(\frac{1}{R_i}-1\right)+\frac{J_v}{k_i} \quad (15)$$

The mass transfer coefficient, k_i can be expressed in term of superficial velocity, U [25]

$$k_i=\alpha_i U^{\beta_i} \quad (16)$$

where α_i and β_i are constants. Substitute Eq. (16) into Eq. (15) becomes

$$\ln\left(\frac{1}{R_{oi}}-1\right)=\frac{J_v}{\alpha_i}\left(\frac{1}{U^{\beta_i}}\right)+\ln\left(\frac{1}{R_i}-1\right) \quad (17)$$

From Eq. (17), a linear relation between the observed rejection expression and $1/U^{\beta_i}$ is obtained when the true rejection expression is held constant. The true rejection can be held constant by measuring the change in observed rejection with varying flow velocity at constant volumetric flux, J_v. The permeate flux can be simply held constant by maintaining a constant operating pressure, high enough to neglect minor osmotic back-pressure effects. The coefficient α_i and β_i are obtained from the best linear fit of data and the intercept of y-axis is the true rejection expression.

3. Experimental

3.1. Sample preparation

The characteristic of POME is shown in Table 1. Table 1 shows that the high content of BOD and COD in POME indicated that the POME has an extremely high content of degradable organic matters, which is due in part to the presence of unrecovered palm oil.

The POME is a very complex mixture of organic matters and all specific components of the organic matters could not be determined. The distribution of chemical constituents of POME has been determined and analyzed by several researchers [1,26,27] and is summarized in Table 1. The high BOD and COD of the POME are contributed by four major groups of organic matters, which are oil and grease, carbohydrate constituents, protein and ammoniacal nitrogen. The oil and grease comprises triglycerides (C46–C56) with the molecular weight of 813–925 kg/kmol where palmitic (44.2 wt.%) and oleic acids (39.2 wt.%) are its main components [28]. The carbohydrate constituents comprise of low molecular weight monosaccharide (180 kg/kmol) to high molecular weight polysaccharide (400,000 kg/kmol). The protein comprises from the simplest compounds of amino acids (75 kg/kmol) to the most complex compounds of proteins (450,000 kg/kmol). Nitrogen in POME is originally present in the form of organic (protein) nitrogen and as time progress, the organic nitrogen is gradually converted to ammoniacal nitrogen which has the molecular weight of 17–35 kg/kmol [27].

Table 1
Characteristic and distribution of chemical constituents of palm oil mill effluent (POME)

Parameter	Concentration
pH	4.7
Oil and grease (mg/L)	4000
Biological oxygen demand (BOD) (mg/L)	25,000
Chemical oxygen demand (COD) (mg/L)	50,000
Total solids (mg/L)	40,500
Suspended solids (mg/L)	18,000
Ammoniacal nitrogen (mg/L)	35
(a) Mineral (mg/L)	3,560
Phosphorous	180
Potassium	2,270
Magnesium	615
Calcium	439
Boron	7.6
Iron	46.5
Manganese	2.0
Copper	0.89
Zinc	2.3
(b) Carbohydrate constituents (mg/L)	3,900
Glucose	140
Reducing sugars	1,450
Starch	360
Pectin	328
Others	1,622
(c) Protein (mg/L)	2,830
Amino acids	Not available
Peptides	Not available
Others	Not available

POME was obtained from the United Palm Oil Mill, Penang, Malaysia. The pretreatment of POME was required to remove the oil and grease and total solids before the POME was fed into the reverse osmosis system [2]. Hundred litres of POME was transferred to a chemical treatment tank for the coagulation and flocculation process. Three litres of coagulant, modified industrial grade alum purchased from Envilab Sdn. Bhd. was added into the POME at the stirring speed of 50 rpm. The pH value was adjusted to the pH 6 by using industrial grade sodium hydroxide 65% (NaOH). Three litres of flocculant (0.1%), cationic polymer (FO 4190) was added into the POME at the stirring speed of 10 rpm for 15 min. The mixture was allowed to settle and the sludge was removed using a filter press. The details of the pretreatment of POME are

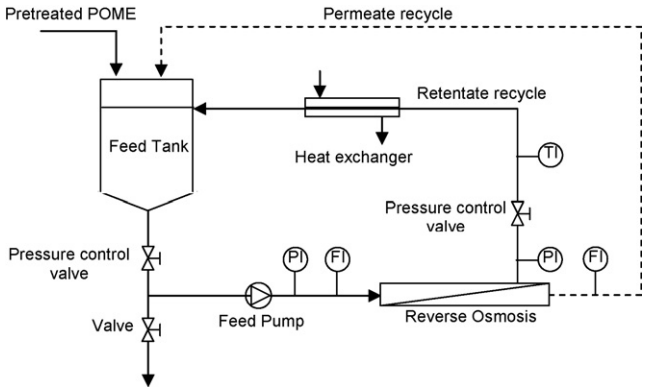

Fig. 3. Schematic diagram of the pilot plant scale equipment set up for reverse osmosis studies. The symbol PI is the pressure indicator, FI is the flowmeter and TI is the temperature indicator.

presented elsewhere [2]. The oil and grease as well as the total solids were removed (with 70% removal of COD) by the coagulation and flocculation processes. The remaining COD (30%) was removed by the ultrafiltration and reverse osmosis processes. The ultrafiltration in this case serves as the pretreatment for reverse osmosis with another 20% removal of the remaining COD. The major components (solutes) contributing to the COD were carbohydrate constituents, protein and ammoniacal nitrogen obtained from the chemical composition analysis of the pretreated POME [1,26]. Therefore, the pretreated POME forms a ternary solutes system for reverse osmosis.

3.2. Membrane system

Fig. 3 shows a schematic diagram of the pilot plant scale set up used in the present study. The reverse osmosis membrane was the PVDF membrane module B1 (PCI-Memtech) with stainless steel (SS 316) housing. The membrane module had a rejection of 99.9% NaCl with 18 flow channels. The inner diameter of each tube was 12.7 mm and its length was 1219.2 mm. The effective area for filtration was 0.90 m^2 and could be operated up to maximum pressure of 60 bar.

The pretreated POME was placed in the feed tank of the membrane system and the temperature was maintained at room temperature (25 °C) using a water cool heat exchanger. The feed was pumped through the membrane module using a piston type pump (CAT). The required cross-flowrate and trans-membrane pressure were adjusted using pressure control valves (Gemu-diaphragm type). The inlet and outlet pressures of the module were measured using the pressure gauges. The turbine function flowmeters (Burkert) were used to measure cross-flowrates of the feed and permeate. The permeate and the retentate streams were recycled back to the feed tank (total recycle mode) to maintain a constant feed concentration. The feed concentration is periodically checked to ensure only very minimal adsorption of solutes onto the membrane surface. In the present study, the measured feed concentration fluctuates within 1% and therefore, the adsorption factor of the membrane is negligible for the present study.

3.3. Analysis

The viscosity of pretreated POME was measured with a Hoeppler falling ball viscometer. The carbohydrate constituents were determined using the colorimetric method with the phenol–sulfuric acid 98% reaction [29]. The protein was measured by using the colorimetric method with a detergent-compatible formulation based on bicinchoninic acid (BCA Protein Assay, Pierce). The ammoniacal nitrogen was determined using Preliminary Distillation Step followed by Titrimetric Method with standard sulfuric acid titrant, 0.02N and the COD was measured by using the Colorimetric Method at wavelength 600 nm with spectrophotometer CECIL 1000 series, Cambridge, UK [30].

4. Results and discussions

In the present study, the experimental data were obtained from the pilot plant scale membrane system with the pretreated POME as the feed to the reverse osmosis module. The pretreated POME was composed of mainly a ternary solutes system (carbohydrate constituents, protein and ammoniacal nitrogen). The concentration of each solute in the feed was 1.625 kg/m^3 for carbohydrate constituents, 0.619 kg/m^3 for protein and 0.028 kg/m^3 for ammoniacal nitrogen, respectively. The combination of these concentrations contributed to the COD value of 12,000 mg/L.

4.1. System parameters

The estimation of parameters for the membrane transport model is an important aspect of this study. Since the composition of the membrane was proprietary, therefore, its material properties were not available. The results from the experimental test of the membrane system were employed for parameter estimation. These parameters were μ, L_p, σ_i, D_{bi}, P_{ii}, and P_{ij}, and their estimated values are listed in Table 2.

Table 2 shows that the viscosity (μ) of pretreated POME as 1.0240×10^{-3} Pa s was slightly higher than the viscosity of water (8.7790×10^{-4} Pa s) due to the presence of organic matters (carbohydrate constituents, protein and ammoniacal nitrogen) in the pretreated POME. Other parameters of L_p, σ_i, D_{bi}, P_{i1}, P_{i2} and P_{i3} matched with their typical values in the literature [13,17,18,31,32]. The solute permeability constants with the consideration of intra-solutes interactions (P_{11}, P_{22} and P_{33}) gave a higher order of magnitude compared to the solute permeability constants with the consideration of inter-solutes interactions (P_{12}, P_{13}, P_{21}, P_{23}, P_{31} and P_{32}). This indicates that in the multiple solutes system, the inter-solutes interactions gave a lower permeability of the particular solute to transport through the membrane compared to the intra-solutes interactions.

4.2. Flux and concentration polarization of the membrane

Fig. 4 shows the volumetric flux of permeate versus filtration time with the increasing trans-membrane pressure varying from 13.5 to 45.0 bar. The feed flowrate and velocity were kept constant at 16 L/min and 7 m/min, respectively. The sim-

Table 2
Estimated parameters for the model

Parameter	Value		
L_p (m/Pa s)	9.0096×10^{-12}		
μ (Pa s)	1.0240×10^{-3}		
	Solute[a]		
	(1) Carbohydrate	(2) Protein	(3) Ammoniacal nitrogen
σ_I	0.9998	0.9999	0.9989
D_{bi} (m^2/s)	3.16×10^{-9}	0.67×10^{-9}	1.54×10^{-9}
P_{i1} (m/s)	7.3456×10^{-9}	7.8428×10^{-14}	4.0616×10^{-13}
P_{i2} (m/s)	2.3672×10^{-13}	1.2162×10^{-8}	1.4840×10^{-12}
P_{i3} (m/s)	3.8432×10^{-12}	3.6334×10^{-12}	1.3969×10^{-7}

[a] The number in front of each solute indicates the solute numbering, which is $i = 1$, 2, and 3.

ulation results show a good agreement with the experimental data with the coefficient of determination (r^2) more than 0.9 for the trans-membrane pressure of 13.5–45.0 bar. Fig. 4 indicates that the fouling of the membrane caused the volumetric flux of permeate to decrease until the system reached a steady-state value. It can be seen that with constant feed concentration of carbohydrate constituents, protein and ammoniacal nitrogen, fractional permeate flux reductions of 17.9, 25.5, 29.0 and 30.8% were experienced, corresponding to trans-membrane pressures of 13.5, 24.5, 35.0 and 45.0 bar, respectively. Although the permeate fluxes were greater at higher trans-membrane pressures (due to the greater driving force), the fractional permeate flux reductions were quantitatively increased at higher trans-membrane pressures. A qualitative explanation for this observed behavior is that at higher trans-membrane pressures, higher concentrations build up in the boundary layer resulted higher wall concentrations and consequently, leading to a higher deterioration rate in permeate flux. However, as depicted from Fig. 4, the volumetric flux of permeate versus filtration time is quite constant with minor deterioration as the maximum fractional permeate flux reductions is 30.8%. This shows that it is adequate to investigate the reverse osmosis filtration of pretreated POME system with concentration polarization phenomena by ignoring the fouling effects.

Fig. 5 depicts the unsteady-state simulation results using the coupled model of concentration polarization and the extended Spiegler-Kedem model. Fig. 5 shows the dependence of wall concentrations for each solute on filtration time. For all the solutes, the wall concentrations increased at the increasing trans-membrane pressure of 13.5–45.0 bar. The wall concentrations increased sharply at the initial filtration time. After a sharp increase during the initial filtration time, this increase became sluggish and gradually approached asymptotic value. Based on the simulation results, the fractional wall concentration increase for each solute corresponding to the increasing trans-membrane pressures are listed in Table 3. The fractional wall concentrations increase for each solute were quantitatively increased at higher trans-membrane pressures, and thus lead to faster concentration build up in the boundary layer and deterioration in permeate flux as shown in Fig. 4. Each solute of carbohydrate constituents, protein and ammoniacal nitrogen show a similar fractional wall concentrations increase (e.g., 5.46, 5.54 and 5.41%, respectively) at the same trans-membrane pressure (e.g., 13.5 bar). This indicates that the fractional wall concentrations for each solute increased at the same rate with the increasing trans-membrane pressure.

The unsteady-state concentration polarization profiles within the boundary layer at the constant trans-membrane pressure of 13.5 bar for each solute of carbohydrate constituents, protein and ammoniacal nitrogen are shown in Fig. 6. All the solutes demonstrate similar trends in concentration polarization where the solute concentrations increased from the initial bulk concentration to the maximum concentration (wall concentration) along the boundary layer in axial direction. Fig. 6(a)–(c) depict that although the wall concentrations increased sharply at the initial filtration time, the initial concentration build up along the boundary layer was sluggish. After a sluggish increase during the initial

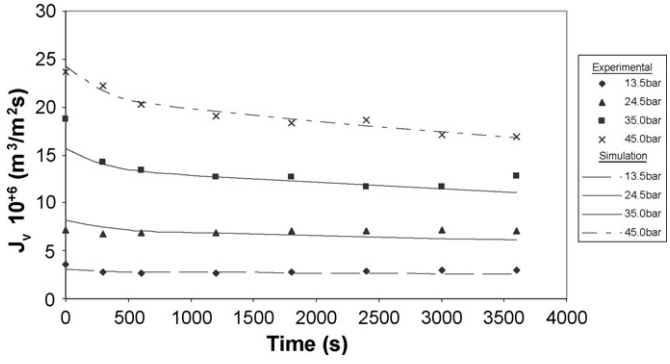

Fig. 4. Volumetric flux of permeate against filtration time at different trans-membrane pressure.

Table 3
Fractional wall concentrations increase for each solute

ΔP (bar)	Solute		
	Carbohydrate constituents (%)	Protein (%)	Ammoniacal nitrogen (%)
13.5	5.46	5.54	5.41
24.5	13.56	13.72	13.72
35.0	25.62	25.90	25.99
45.0	41.30	41.73	41.88

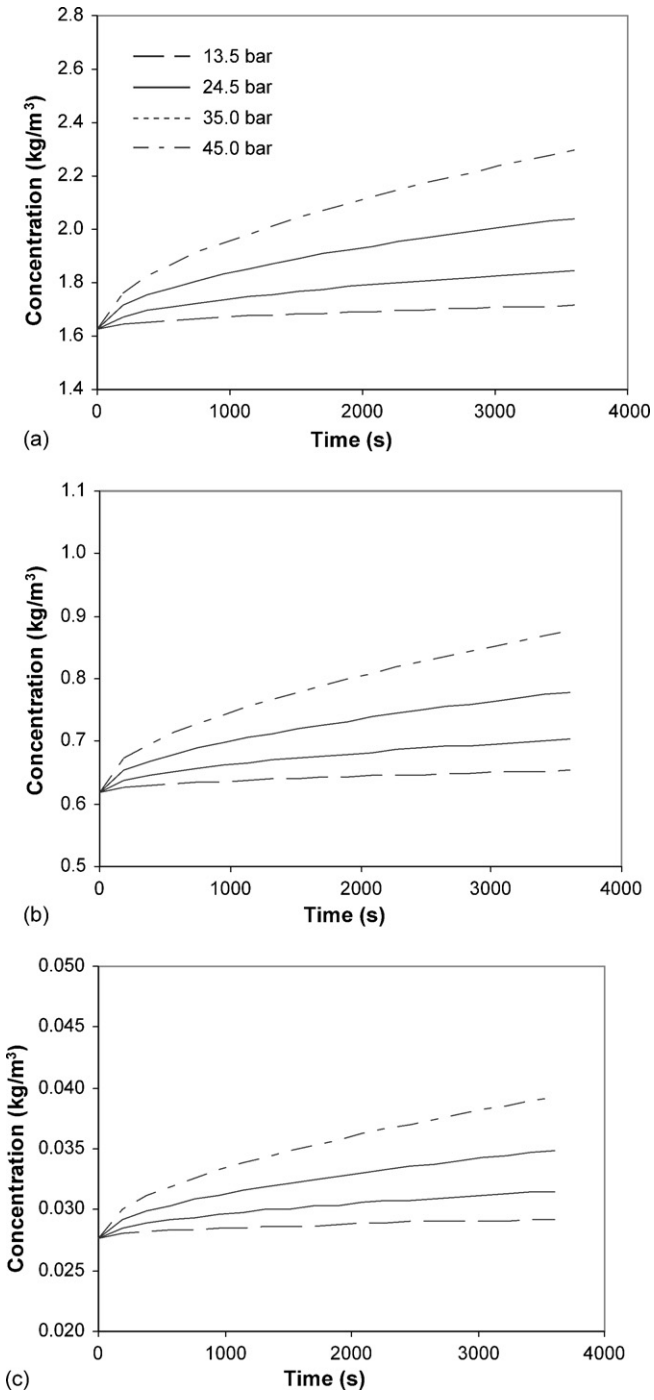

Fig. 5. Simulation results of wall concentrations for (a) carbohydrate constituents (b) protein and (c) ammoniacal nitrogen against filtration time.

filtration time, the concentrations build up along the boundary layer became greater despite a sluggish wall concentration increase. It must be noted that at initial filtration time, there was no accumulation of rejected solutes along the boundary layer. As filtration progress, the amount of rejected solutes was gradually increased and consequently lead to higher wall concentration and back-diffusion mass transfer rate into the boundary layer. The accumulation of back transported solutes resulted greater concentrations build up along the boundary layer.

4.3. Permeate quality for the ternary solutes system

The outcome of the experiment demonstrates that the reverse osmosis membranes were able to reject the complex organic matters effectively with the minimum observed rejection of

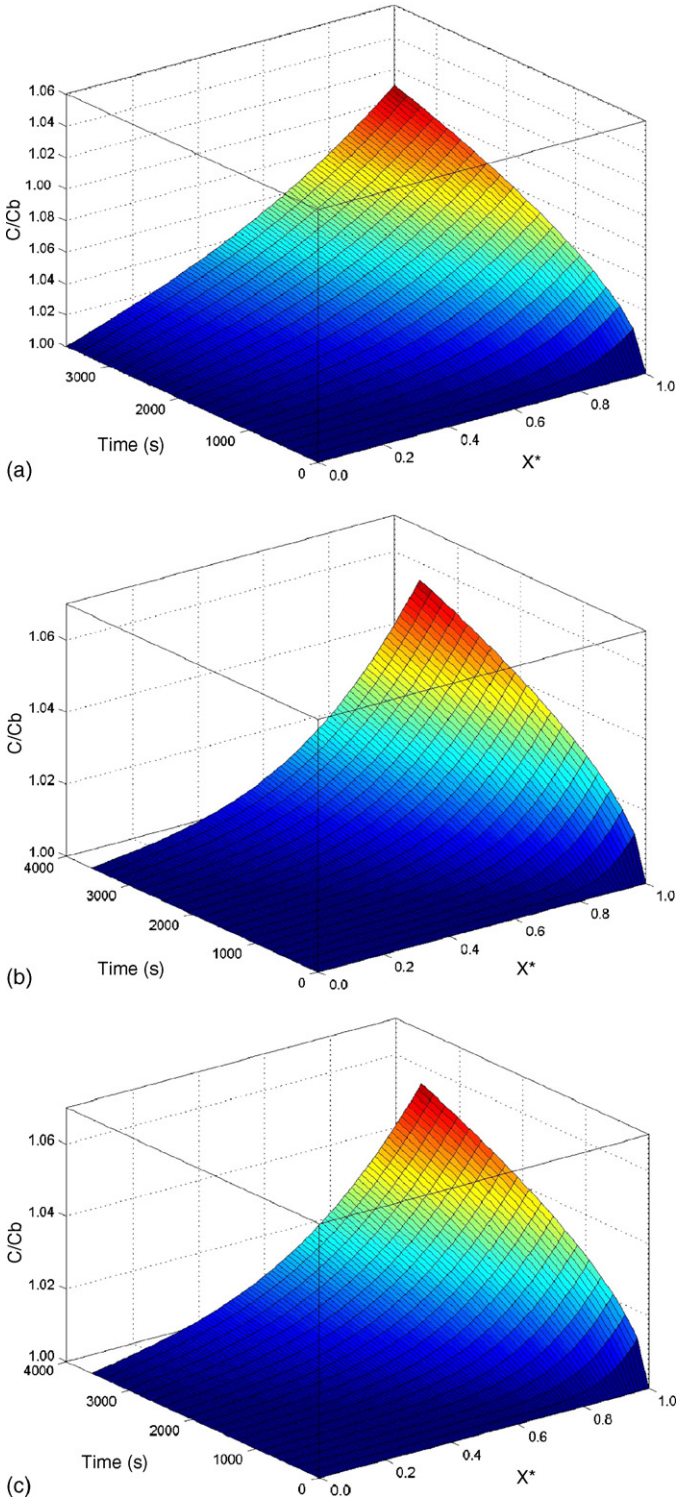

Fig. 6. Simulation results of concentration buildup profile for (a) carbohydrate constituents (b) protein and (c) ammoniacal nitrogen along the concentration polarization boundary layer against filtration time.

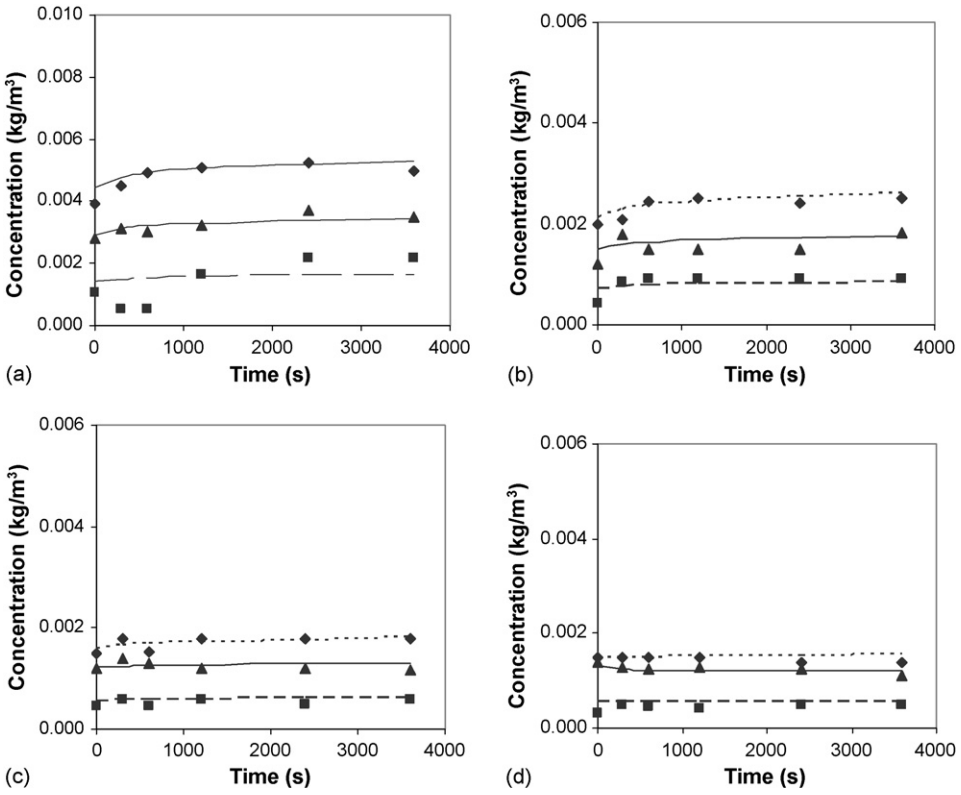

Fig. 7. The unsteady-state permeate concentration for each solutes at trans-membrane pressure of (a) 13.5 bar (b) 24.5 bar (c) 35.0 bar and (d) 45.0 bar. The symbols (♦), (▲) and (■) indicate the experimental results for carbohydrate constituents, protein and ammoniacal nitrogen, respectively. The symbols (- - -), (—) and (— —) indicate the simulation results for carbohydrate constituents, protein and ammoniacal nitrogen, respectively.

0.996, 0.994 and 0.921 for carbohydrate constituents, protein and ammoniacal nitrogen, respectively. The higher molecular weight of solutes (carbohydrate constituents and protein) gave a higher observed rejection compared to the solute which had the lower molecular weight (ammoniacal nitrogen). The simulation and experimental results of permeate concentrations for each solute (carbohydrate constituents, protein and ammoniacal nitrogen) against filtration time at the increasing trans-membrane pressure of 13.5–45.0 bar is shown in Fig. 7. The simulation results showed a good agreement with the experimental data.

Fig. 7(a)–(d) depict a similar trend of lower permeate concentrations for each solutes when the trans-membrane pressure increased. This phenomenon resulted higher observed rejection for each solutes at higher trans-membrane pressure due to the higher driving force which would force more solvent (water) to diffuse through the membrane. The simulation results of Fig. 7(a)–(d) show that the permeate concentration for each solutes increased slightly from the initial filtration time until the steady-state condition was reached. The behavior observed from Fig. 7(a)–(d) shows that the observed rejection decreased slightly from the initial filtration time until the steady-state condition was reached.

Fig. 8 shows the unsteady-state simulation results of intrinsic rejection for each solute of carbohydrate constituents, protein and ammoniacal nitrogen at increasing trans-membrane pressure. All solutes demonstrate an identical behavior where the intrinsic rejection increased with the increasing trans-membrane pressure and filtration time. The observed behavior clearly demonstrates the importance of concentration polarization and the efficiency of reverse osmosis to reject the organic matters on the intrinsic rejections. The concentration polarization factor as shown in Fig. 6 contributed to accumulation of solutes on the membrane wall (Fig. 5). However, the reverse osmosis membranes maintained relatively constant observed rejections for each solute with only slight increase of permeate concentrations as shown in Fig. 7. Therefore, the reverse osmosis membranes effectively retained the organic solutes regardless to the extent of concentration polarization and consequently, contributed to the increase in intrinsic rejection with filtration time.

The correlation in the present study related the concentrations of all solutes ($C_{p,carbohydrate}$, $C_{p,protein}$, $C_{p,nitrogen}$) with the COD value in the membrane system. The correlation was obtained by using the multivariable regression of Levenberg–Marquardt method. The values of the dimensionless coefficients b_1, b_2 and b_3 were 0.3535, 4.9279 and 0.5595, respectively obtained using Eq. (10). The final correlation is given by Eq. (18).

$$COD_{calculated} = 0.3535C_{p,carbohydrate} + 4.9279C_{p,protein} + 0.5595C_{p,nitrogen} \quad (18)$$

The comparison of the experimental data and the model predictions is shown in Fig. 9. It shows that the correlation was successfully applied in the prediction of COD value in the membrane system with the coefficient of determination (r^2) of 0.9911.

The simulation values obtained from Eq. (18) showed a good fit with the experimental data as demonstrated in Fig. 10. Fig. 10

demonstrates a decrease of COD reading in the permeate stream when the trans-membrane pressure increased. This was in line with the permeate concentration shown in Fig. 7. The decrease of permeate concentration at the increasing trans-membrane pressure resulted more solvent to diffuse through membrane, and thus lower COD reading was obtained.

The low COD reading in the permeate stream compared to the COD reading in the feed stream (12,000) shows that the

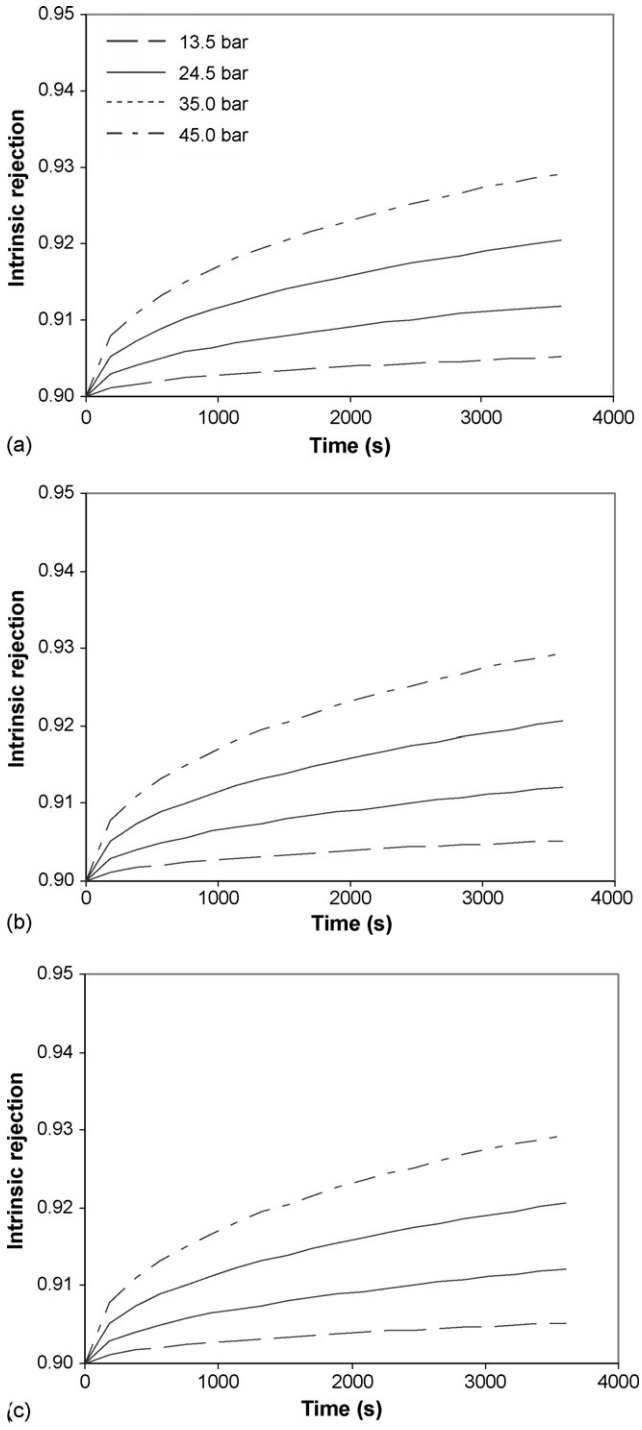

Fig. 8. Unsteady-state simulation results of intrinsic rejections for (a) carbohydrate constituents (b) protein and (c) ammoniacal nitrogen for increasing trans-membrane pressure.

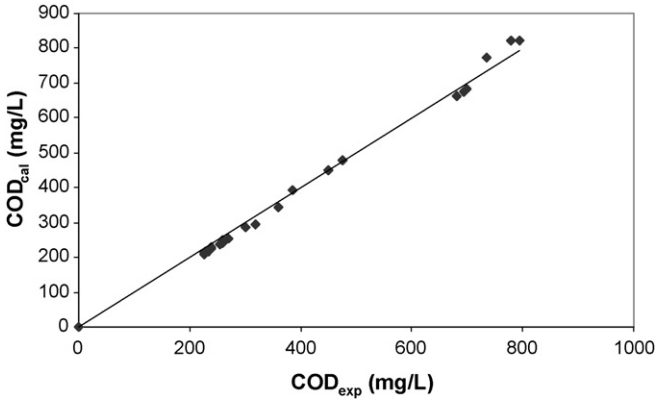

Fig. 9. Comparison of experimental COD against calculated COD.

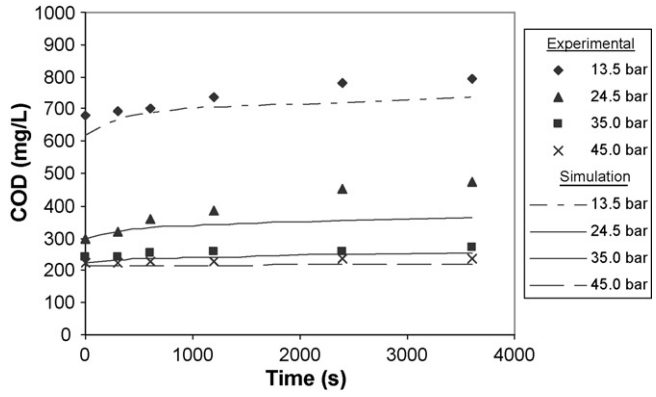

Fig. 10. Variation of unsteady-state COD reading in the permeate with increasing trans-membrane pressure.

efficiency of COD removal using reverse osmosis was high (94–98% of COD removal). The high rejection of carbohydrate constituents, protein and ammoniacal nitrogen indicated that most of the solutes were unable to diffuse through the membrane, and thus contributed to high efficiency of COD removal.

5. Conclusion

A membrane transport model suitable for the multiple solutes system in reverse osmosis based on the coupled model of concentration polarization using unsteady-state differential material balance and extended Spiegler-Kedem model has been developed. The comparisons between the proposed model and the experimental data of ternary solutes system (pretreated POME) for the reverse osmosis showed a good agreement and proved its utility in predicting the performance of the multiple solutes system.

The proposed model successfully predicted the volumetric permeate flux decline and the concentration polarization for each solute as a function of filtration time. In addition, the proposed model demonstrated a good predicting capability of permeate concentrations and intrinsic rejections of each solute of the system. The correlation for the concentrations of all solutes with the COD value in the permeate stream of the membrane system has been successfully developed. In overall, a method of predicting the performance of reverse osmosis using complex

organics solutions by applying the coupled model of concentration polarization and extended Spiegler-Kedem model with the consideration of solute–solute interactions has been successfully developed.

The reverse osmosis gave high efficiency of COD removal for pretreated POME due to the high rejection of carbohydrate constituents, protein and ammoniacal nitrogen. Thus, the reverse osmosis is effective to remove the remaining micromolecules in the pretreated POME to achieve the desired water quality.

Acknowledgements

The authors would like to gratefully acknowledge Federal Land Development Authority Foundation (Yayasan Felda) of Malaysia for their financial support. The authors would also like to thank United Oil Palm Industry, Nibong Tebal, Pulau Pinang for providing the sample of POME to conduct this research.

References

[1] T.K. Hwang, S.M. Ong, C.C. Seow, H.K. Tan, Chemical composition of palm oil mill effluents, Planter 54 (1978) 749.
[2] A.L. Ahmad, S. Ismail, S. Bhatia, Water recycling from palm oil mill effluent (POME) using membrane technology, Desalination 157 (2003) 87.
[3] A. Abbas, Simulation and analysis of an industrial water desalination plant, Chem. Eng. Process. 44 (2005) 999.
[4] M. Taniguchi, S. Kimura, Estimation of transport parameters of RO membranes for seawater desalination, AIChE J. 46 (2000) 10.
[5] B. Mi, C.L. Eaton, J.H. Kim, C.K. Colvin, J.C. Lozier, B.J. Mariñas, Removal of biological and non-biological viral surrogates by spiral-wound reverse osmosis membrane elements with intact and compromised integrity, Water Res. 38 (2004) 3821.
[6] K. Kimura, S. Toshima, G. Amy, Y. Watanabe, Rejection of neutral endocrine disrupting compounds (EDCs) and pharmaceutical active compounds (PhACs) by RO membranes, J. Membr. Sci. 245 (2004) 71.
[7] L.D. Nghiem, A. Manis, K. Soldenhoff, A.I. Schäfer, Estrogenic hormone removal from wastewater using NF/RO membranes, J. Membr. Sci. 242 (2004) 37.
[8] H. Strathmann, Membrane separation processes: current relevance and future opportunities, AIChE J. 47 (2001) 5.
[9] M. Turan, Influence of filtration conditions on the performance of nanofiltration and reverse osmosis membranes in dairy wastewater treatment, Desalination 170 (2004) 83.
[10] J. Bohdziewicz, E. Sroka, Integrated system of activated sludge-reverse osmosis in the treatment of the wastewater from the meat industry, Process Biochem. 40 (2005) 1517.
[11] J.J. Qin, M.H. Oo, M.N. Wai, H. Lee, S.P. Hong, J.E. Kim, Y. Xing, M. Zhang, Pilot study for reclamation of secondary treated sewage effluent, Desalination 171 (2004) 299.
[12] E. Darnon, M.P. Belleville, G.M. Rios, Modeling ultrafiltration of complex biological solutions, AIChE J. 48 (2002) 8.
[13] N. Al-Bastaki, Removal of methyl orange dye and Na_2SO_4 salt from synthetic waste water using reverse osmosis, Chem. Eng. Process. 43 (2004) 1561.
[14] K.M. Pastagia, S. Chakraborty, S. DasGupta, J.K. Basu, S. De, Prediction of permeate flux and concentration of two-component dye mixture in batch nanofiltration, J. Membr. Sci. 218 (2003) 195.
[15] S.C. Tu, V. Ravindran, W. Den, M. Pirbazari, Predictive membrane trasport model for nanofiltration processes in water treatment, AIChE J. 47 (2001) 6.
[16] S.K. Karode, Unsteady state flux response: a method to determine the nature of the solute and gel layer in membrane filtration, J. Membr. Sci. 188 (2001) 9.
[17] A.L. Ahmad, M.F. Chong, S. Bhatia, Mathematical, Modeling and simulation of the multiple solutes system for nanofiltration process, J. Membr. Sci. 253 (2005) 103.
[18] S. Wadley, C.J. Brouckaert, L.A.D. Baddock, C.A. Buckley, Modelling of nanofiltration applied to the recovery of salt from waste brine at a sugar decolourisation plant, J. Membr. Sci. 102 (1995) 163.
[19] A. Bhattacharya, P. Ghosh, Nanofiltration and reverse osmosis membranes: theory and application in separation of electrolytes, Rev. Chem. Eng. 20 (2004) 111.
[20] A.F. Miorin, Wastewater Treatment Plant Design, Water Pollution Control Federation, USA, 1977.
[21] S.C. Chapra, R.P. Canale, Numerical Methods for Engineers, McGraw-Hill, New York, 1998.
[22] R.D. Skeel, M. Berzins, A method for the spatial discretization of parabolic equations in one space variable, SIAM J. Sci. Stat. Comput. 11 (1990) 1.
[23] S. Jain, S.K. Gupta, Analysis of modified surface pore flow model with concentration polarization and comparison with Spiegler-Kedem model in reverse osmosis system, J. Membr. Sci. 232 (2004) 45–61.
[24] I. Sutzkover, D. Hasson, R. Semiat, Simple technique for measuring the concentration polarization level in a reverse osmosis system, Desalination 131 (2000) 117.
[25] W.R. Baker, Membrane Technology and Applications, Membrane Technology and Research Inc., California, 1997.
[26] C.C. Ho, Y.K. Tan, C.W. Wang, The distribution of chemical constituents between the soluble and the particulate fractions of palm oil mill effluent and its significance on its utilization/treatment, J. Agric. Wastes 11 (1984) 61.
[27] M.C. Chow, Palm Oil Mil Effluent Analysis, Palm Oil Research Institute of Malaysia, Kuala Lumpur, 1991, pp. 11–18.
[28] B.K. Tan, O.S.H. Augustine, O.C.H. Flingoh, Effects of composition on palm oil properties, PORIM Bull. 3 (1981) 14.
[29] M. Dubois, K.A. Gilles, J.K. Hamilton, P.A. Rebers, F. Smith, Colorimetric method for determination of sugars and related substances, Anal. Chem. 28 (1956) 350.
[30] American Public Health Association (APHA), Standard Methods for the Examination of Water and Wastewater, APHA, Washington, DC, 1999.
[31] C.J. Geankoplis, Transport Processes Unit Operations, 3rd ed., Prentice-Hall International Inc., New Jersey, 1993.
[32] J.G. Albright, O. Annunziata, D.G. Miller, L. Paduano, A.J. Pearlstein, Precision measurements of binary and multicomponent diffusion coefficients in protein solutions relevant to crystal growth: lysozyme chloride in water and aqueous NaCl at pH 4.5 and 25 °C, J. Am. Chem. Soc. 121 (1999) 3256–3266.